PCCP

ROYAL SOCIETY OF CHEMISTRY

PAPER

View Article Online
View Journal | View Issue

Cite this: *Phys. Chem. Chem. Phys.*, 2024, **26**, 16674

Insights into the baicalein-induced destabilization of LS-shaped $A\beta_{42}$ protofibrils using computer simulations†

Gagandeep Kaur,‡[a] Opinder Kaur Mankoo, ‡[a] Anupamjeet Kaur,§[a] Deepti Goyal *[b] and Bhupesh Goyal *[c]

Amyloid-β (Aβ) peptides aggregate spontaneously into various aggregating species comprising oligomers, protofibrils, and mature fibrils in Alzheimer's disease (AD). Disrupting β-sheet rich neurotoxic smaller soluble $A\beta_{42}$ oligomers formed at early stages is considered a potent strategy to interfere with AD pathology. Previous experiments have demonstrated the inhibition of the early stages of Aβ aggregation by baicalein; however, the molecular mechanism behind inhibition remains largely unknown. Thus, in this work, molecular dynamics (MD) simulations have been employed to illuminate the molecular mechanism of baicalein-induced destabilization of preformed $A\beta_{42}$ protofibrils. Baicalein binds to chain A of the $A\beta_{42}$ protofibril through hydrogen bonds, π–π interactions, and hydrophobic contacts with the central hydrophobic core (CHC) residues of the $A\beta_{42}$ protofibril. The binding of baicalein to the CHC region of the $A\beta_{42}$ protofibril resulted in the elongation of the kink angle and disruption of K28–A42 salt bridges, which resulted in the distortion of the protofibril structure. Importantly, the β-sheet content was notably reduced in $A\beta_{42}$ protofibrils upon incorporation of baicalein with a concomitant increase in the coil content, which is consistent with ThT fluorescence and AFM images depicting disaggregation of pre-existing $A\beta_{42}$ fibrils on the incorporation of baicalein. Remarkably, the interchain binding affinity in $A\beta_{42}$ protofibrils was notably reduced in the presence of baicalein leading to distortion in the overall structure, which agrees with the structural stability analyses and conformational snapshots. This work sheds light on the molecular mechanism of baicalein in disrupting the $A\beta_{42}$ protofibril structure, which will be beneficial to the design of therapeutic candidates against disrupting β-sheet rich neurotoxic $A\beta_{42}$ oligomers in AD.

Received 10th December 2023,
Accepted 15th May 2024

DOI: 10.1039/d3cp06006c

rsc.li/pccp

[a] *Department of Chemistry, Faculty of Basic and Applied Sciences, Sri Guru Granth Sahib World University, Fatehgarh Sahib-140406, Punjab, India*
[b] *Department of Chemistry, DAV College, Sector 10, Chandigarh-160011, India. E-mail: deeptig@iitbombay.org*
[c] *Department of Chemistry & Biochemistry, Thapar Institute of Engineering & Technology, Patiala-147004, Punjab, India. E-mail: bhupesh@iitbombay.org*

† Electronic supplementary information (ESI) available: Input conformation of the $A\beta_{42}$ protofibril and baicalein for molecular docking, the top nine docked conformations of baicalein with the $A\beta_{42}$ protofibril, 2D interaction maps displaying hydrophobic contacts of baicalein with the $A\beta_{42}$ protofibril in the top nine docked conformations, the correlation between simulation (δ_{sim}) and experimental (δ_{exp}) NMR data of the $A\beta_{42}$ protofibril, RMSF of each chain of protofibril during the simulation, RMSF and R_g variations in repeat simulations, modulation of contacts in the hydrophobic core of 5OQV on the inclusion of baicalein, kink angle distribution, and K28–A42 salt bridge distribution are shown in Fig. S1–S10. The molecular docking results, $A\beta_{42}$ protofibril residues involved in intermolecular hydrophobic contacts with baicalein in the top nine docked poses, hydrogen bonds between H6–E11 and E11–H13 of the $A\beta_{42}$ protofibril, and secondary structure composition of the control and baicalein systems for repeat simulations are reported in Tables S1–S4. See DOI: https://doi.org/10.1039/d3cp06006c

‡ Both authors contributed equally to this manuscript.

§ Present address: National Institute of Immunology, Aruna Asaf Ali Marg, New Delhi–110067, India.

1. Introduction

Alzheimer's disease (AD) is a neurodegenerative disease marked by progressive cognitive decline and memory loss along with changes in behavioural and social abilities.[1] According to Alzheimer's Disease International, dementia affects ~55 million people globally with the prevision of becoming 139 million by 2050.[2] AD is characterized by an extracellular abnormal protein accumulation called amyloids[3] and intracellular neurofibrillary tangles in the brain. In AD, the amyloids are composed of β-sheet rich neurotoxic fibrillar aggregates of amyloid-β (Aβ).[4] Aβ is a 39 to 42 amino acid peptide produced from the cleavage of amyloid precursor protein (APP) by β- and γ-secretases. Aβ being an intrinsically disordered protein, numerous U-shaped,[5] S-shaped,[6] and LS-shaped[7] Aβ oligomers with two-fold or three-fold symmetry[8] have been reported as cytotoxic species.[9]

Currently, FDA-approved drugs such as galantamine, rivastigmine, and donepezil are cholinesterase inhibitors and provide only temporary relief from the symptoms of AD. Thus, there is a

requirement for new drug candidates that can inhibit or reverse AD progression. Since the deposition of Aβ is intimately linked to the onset of AD pathogenesis, targeting Aβ aggregation is considered a key therapeutic strategy against AD.[10] Furthermore, the recent approval of the humanized IgGI monoclonal antibody lecanemab by the FDA for treating AD in its early stages has sparked interest in the development of new chemical entities (NCEs) against Aβ aggregation.[11]

The application of small molecules, particularly polyphenols and flavonoids, to target different aggregated species generated during the aggregation pathway has emerged as a promising approach. The phenolic hydroxyl groups and phenyl rings in polyphenols or flavonoids interact with the hydrophobic residues and aromatic groups present in the amyloidogenic proteins and inhibit the self-aggregation of proteins.[12] Baicalein (5,6,7-trihydroxy flavone), a naturally occurring flavonoid obtained from the herb *Scutellaria baicalensis* Georgi, has been explored for its anti-aggregation behaviour against Aβ peptide,[13] α-synuclein,[14] superoxide dismutase I (SOD1)[15] and lysozyme.[16]

Recently, experimental studies have highlighted the key role of baicalein in modulating neurotoxicity induced by Aβ aggregates. In 2011, Lu *et al.* reported that baicalein inhibited Aβ fibrillation and oligomerization, disaggregated the pre-assembled amyloid fibrils, and alleviated the neurotoxicity induced by Aβ aggregates.[13] The fluorescence intensity of thioflavin T (ThT) was almost completely inhibited when $A\beta_{42}$ was co-incubated with 30 μM baicalein and $A\beta_{42}$ fibrillation was inhibited in a dose-dependent manner (IC_{50} = 1.35 μM). Furthermore, baicalein disaggregated the preformed $A\beta_{42}$ fibrils to an amorphous state as demonstrated using electron microscopy. Baicalein rescued PC12 cells from $A\beta_{42}$ induced cytotoxicity (the cell viability was 43.5% at 15 μM concentration of $A\beta_{42}$) in a dose-dependent manner and the cell viability increased to 67% at 30 μM concentration of baicalein. As shown from the atomic force microscopy (AFM) images, when $A\beta_{42}$ is incubated with baicalein, the globular crystalloid aggregates of $A\beta_{42}$ become smaller and long fibrils dissociate into globular deposits, highlighting the disaggregation effect of baicalein.[17] Another study by Wang and coworkers reported that baicalein rescued synaptic plasticity and memory loss in the AD mouse model.[18]

Despite its noteworthy properties, the binding interactions of baicalein on Aβ oligomers and the molecular mechanism of Aβ fibril destabilization remain elusive. Thus, in this work, the disruptive ability of baicalein on Aβ protofibrils was examined using molecular dynamics (MD) simulations. Complementary to experiments, MD simulations illuminate underlying key interactions between proteins and small-molecule inhibitors and are widely employed to illuminate the binding interactions and molecular mechanism of protofibril destabilization of various small molecules.[19] Zheng and coworkers reported that tanshinone I and tanshinone IIA block Aβ protofibril association into fibrillar aggregates by preferentially binding to the hydrophobic β-sheet groove created by residues spanning the C-terminal regions I31–M35 and M35–V39 and various aromatic residues of the U-shaped Aβ pentamer.[20] Using coarse-grained MD simulations, Wang *et al.* demonstrated the distinct inhibitory effects of epigallocatechin gallate (EGCG), resveratrol, curcumin, and vanillin on $A\beta_{17-36}$ aggregation.[21] Martin *et al.* examined curcumin-induced $A\beta_{9-40}$ protofibril destabilization using all-atom MD simulations and reported that curcumin blocked Aβ fibrillization by attaching to hydrophobic regions on the protofibril surface.[22] Gupta and Dasmahapatra depicted that caffeine altered the $A\beta_{17-42}$ protofibrils by weakening the D23–K28 salt bridges and hydrophobic contacts between A21–V36 and F19–G38.[23] Zhan *et al.* employed all-atom MD simulations to demonstrate that EGCG and epigallocatechin (EGC) disrupt Aβ protofibrils with EGCG having a stronger disruptive potential than EGC due to the presence of a gallic acid ester group in EGCG.[24]

To the best of our knowledge, no study has illuminated the molecular mechanism of destabilization of recently cryogenic electron microscopy (cryo-EM) resolved LS-shaped Aβ protofibrils (PDB ID: 5OQV) by baicalein using MD simulations. The key insights from the baicalein-induced destabilization of LS-shaped Aβ protofibrils in this work will inspire the development of NCEs against Aβ aggregates and other cytotoxic oligomeric species implicated in chronic amyloid diseases.

2. Computational details

2.1 Molecular docking

The $A\beta_{42}$ fibril (PDB ID: 5OQV) resolved using cryo-EM was employed in this work to model the protofibril (Fig. 1(a)).[7] The 5OQV structure comprises two intertwined protofibrils, a tetramer and pentamer, with LS-shaped morphology. The $A\beta_{42}$ tetramer was chosen as a model for $A\beta_{42}$ protofibrils in this work as it has been reported as the minimal nucleus of $A\beta_{42}$ protofibrils.[24] Furthermore, a previous experimental work highlighted that the $A\beta_{42}$ tetramer can eliminate the lag phase during fibril elongation.[25] Molecular docking was performed using AutoDock Vina, and a grid box with dimensions 98 × 112 × 80 $Å^3$ was employed for $A\beta_{42}$ protofibrils. PyMOL[26] and Ligplot+[27] were employed to visualize the docking poses and identify $A\beta_{42}$ protofibril residues displaying interactions with baicalein (Fig. 1(b)).

2.2 Details of MD simulations

Two isolated systems, $A\beta_{42}$ protofibril (designated as control) and $A\beta_{42}$ protofibril–baicalein complex (designated as baicalein), were employed for all-atom MD simulations using the AMBER99SB-ILDN[28] force field in GROMACS[29] software (Table 1). The force field parameters of baicalein were generated using ATB (Automated Topology Builder).[30] The $A\beta_{42}$ protofibril was positioned in the centre of a cubic box[19c,31] (8.55 nm × 8.55 nm × 8.55 nm) with a minimum of 1.0 nm distance between the solute and box edges. The overall neutrality at physiological pH was maintained by adding 0.15 M NaCl to each system. Following energy minimization, the control and baicalein systems were solvated with 19 677 and

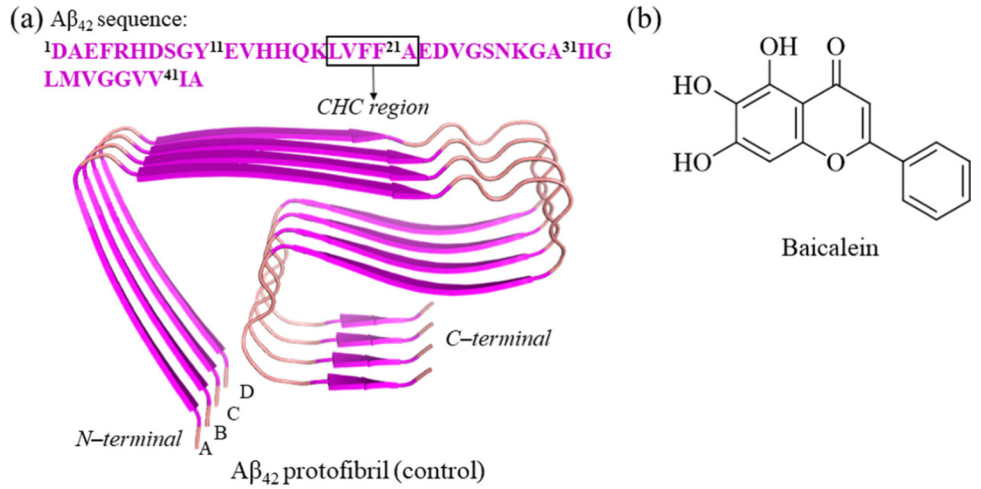

Fig. 1 Structural illustration of the LS-shaped $A\beta_{42}$ protofibril (PDB ID: 5OQV) in a cartoon (panel (a)). The chemical structure of baicalein is shown in panel (b).

Table 1 System details for MD simulations

System	Simulation length[b] (ns)	Box dimensions (nm)	TIP3P water molecules
Control[a]	500 × 2	8.5 × 8.5 × 8.5	19 677
Baicalein	500 × 2	8.5 × 8.5 × 8.5	19 664

[a] $A\beta_{42}$ protofibril (PDB ID: 5OQV). [b] AMBER99SB-ILDN force field was employed in the simulations.

19 664 transferable intermolecular potential with 3 point (TIP3P)[32] water molecules, respectively. The particle mesh Ewald (PME) method was employed to treat long-range electrostatic interactions.[33] The systems were equilibrated for 500 ps in the NVT ensemble and 500 ps in the NPT ensemble after energy minimization by the steepest descent method. Using a Parrinello–Rahman barostat[34] and a velocity rescale thermostat,[35] an MD simulation of length 500 ns was performed for each system at 1 bar and 310 K.

2.3 MD analysis

Several GROMACS tools were used to analyze the MD trajectories. The analyses have been performed on the last 400 ns of the MD trajectories. The structural changes in $A\beta_{42}$ protofibrils upon incorporation of baicalein were monitored using *gmx rmsf*. The radius-of-gyration (R_g) was determined using *gmx gyrate*. The effect of baicalein on the secondary structure of $A\beta_{42}$ protofibrils was assessed using the dictionary of the secondary structure of proteins (DSSP).[36] The conformations were determined using the *gmx cluster* by employing the Daura *et al.* algorithm.[37] The contacts between $A\beta_{42}$ residues with and without baicalein were examined using the *gmx mdmat* tool.

The molecular mechanics Poisson–Boltzmann surface area (MM-PBSA) approach was used to determine the binding affinity of baicalein with $A\beta_{42}$ protofibrils using the GROMACS tool *g_mmpbsa*.[38] Furthermore, residue-wise interactions and interchain binding free energy analyses were performed using *g_mmpbsa*. The relative binding free energy of the $A\beta_{42}$ protofibril–baicalein complex was evaluated. The absolute binding free energy is overestimated by MM-PBSA; however, the relative binding affinities are adequate. Thus, following prior computational studies, the binding free energy was determined without taking into account conformational entropy. The NMR chemical shifts of the Cα and Cβ atoms of the central member of the first microstate (m_1) of $A\beta_{42}$ protofibrils were evaluated using SHIFTX2.[39] The chemical shifts of $A\beta_{42}$ protofibrils from the biological magnetic resonance data bank were compared with the values obtained from the simulation.[7,40] The three bond *J*-coupling ($^3J_{NH-H\alpha}$) constants between the amide proton and the Hα atom were evaluated as previously described[41] and compared with experimental $^3J_{NH-H\alpha}$ values.

3. Results and discussion

3.1 Decoding the binding interactions of baicalein with $A\beta_{42}$ protofibrils

The binding regions of baicalein on $A\beta_{42}$ protofibrils were examined using molecular docking. Baicalein was situated away from the aggregation-prone central hydrophobic core[42] (CHC) region of $A\beta_{42}$ protofibrils in the input conformation for molecular docking (Fig. S1(a), ESI†). Baicalein moves and binds to the residues of the CHC region of chain A of $A\beta_{42}$ protofibrils in the best-docked pose with a binding energy of −6.9 kcal mol^{-1} (Fig. S1(b) and Table S1, ESI†). The analysis of the top nine docked poses highlights that baicalein binds to nearly the same region (CHC region of chain A) of $A\beta_{42}$ protofibrils in all poses with binding energies ranging from −6.9 to −5.4 kcal mol^{-1} (Fig. S2, S3, and Table S2, ESI†). In the best-docked pose, the oxygen atom of OH(4) and the hydrogen atom of OH(5) of baicalein display hydrogen bonding interactions with the backbone NH and CO, respectively, of Glu22(A) of $A\beta_{42}$ protofibrils (Fig. 2(a)). Baicalein displays π–π interactions with the CHC region residue Phe19(A).[43] Baicalein

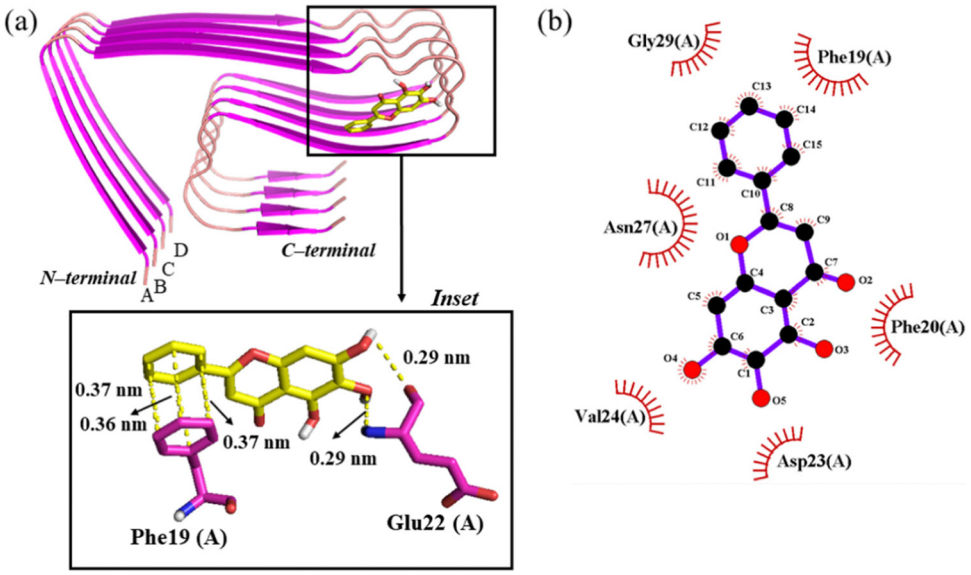

Fig. 2 Binding pose of baicalein (sticks) on $A\beta_{42}$ protofibrils (cartoon) with hydrogen bonds and $\pi-\pi$ interactions shown in the inset (panel (a)). Hydrophobic contacts of baicalein with $A\beta_{42}$ protofibrils (panel (b)).

displays hydrophobic contacts with Phe19(A), Phe20(A), Asp23(A), Val24(A), Asn27(A) and Gly29(A) of $A\beta_{42}$ protofibrils (Fig. 2(b)).

3.2 Validation of conformational ensembles by MD using NMR data

To validate the simulation data, the conformational ensemble of the $A\beta_{42}$ protofibril was compared with the NMR data. The chemical shifts of Cα and Cβ atoms from the simulation data agree well with the observed NMR chemical shifts (R^2 = 0.92 for Cα and 0.96 for Cβ) [Fig. S4(a) and (b), ESI†]. Gong *et al.* reported similar correlation coefficients for Cα atoms (R^2 = 0.88) and Cβ atoms (R^2 = 0.96).[44] Additionally, the average $^3J_{NH-H\alpha}$ coupling constant value from MD simulations is nearly identical to the experimental $^3J_{NH-H\alpha}$ value[6a] (Fig. S4(c), ESI†). The chemical shifts and $^3J_{NH-H\alpha}$ coupling constant values generated from the MD simulation data match well with experimental values.

3.3 Impact of baicalein on the structural stability of $A\beta_{42}$ protofibrils

The root-mean-square fluctuation (RMSF) analysis depicts a notably higher average value of 0.28 ± 0.01 nm in baicalein as compared to 0.15 ± 0.02 nm in the control (Fig. 3(a)), which highlights higher conformational fluctuations in the protofibril system leading to lower overall stability. Furthermore, higher fluctuations were noted in each chain of $A\beta_{42}$ protofibrils on the incorporation of baicalein (Fig. S5, ESI†). Notably, residues 20–30 of chain A displayed significant fluctuations depicting the pronounced effect of baicalein on chain A of the $A\beta_{42}$ protofibrils (Fig. S5(b), ESI†).

Furthermore, the compactness of the protofibril structure was significantly altered with the addition of baicalein (Fig. 3(b)). A higher radius-of-gyration (R_g) value of 1.56 ± 0.14 nm in baicalein as compared to 1.46 ± 0.09 nm in the control indicates the loosening of the well-packed chains in the protofibril. Thus, notably higher RMSF and R_g values in the baicalein system depict

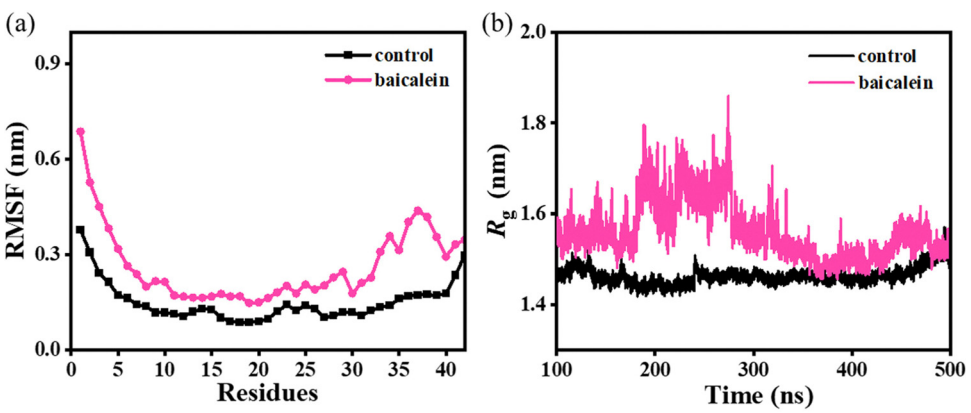

Fig. 3 Average RMSF (panel (a)) and variations in R_g (panel (b)) in the control and baicalein systems.

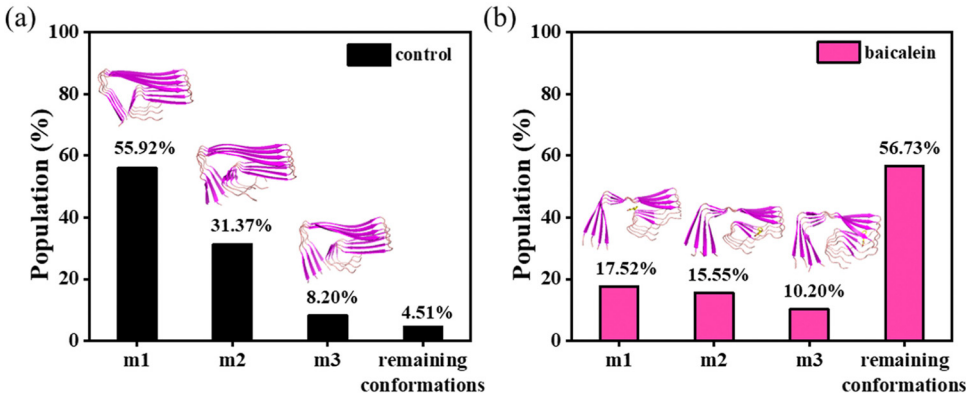

Fig. 4 Conformational sampling in the first three microstates with central members in a cartoon for the control (panel (a)) and baicalein (panel (b)) systems.

a reduced stability of the protofibril structure. Similar RMSF and R_g values were noted in the replicates with random initial velocities, which highlight the repeatability and reproducibility of the simulation data (Fig. S6 and S7, ESI†).

The conformational sampling in the first two microstates was remarkably decreased from 55.92 and 31.37% in the control to 17.52 and 15.55%, respectively, in baicalein, which indicates conformational heterogeneity in $A\beta_{42}$ protofibrils on the addition of baicalein (Fig. 4).

Baicalein displayed hydrogen bonds and hydrophobic contacts with the residues (region 15–34) of $A\beta_{42}$ protofibrils in the central member of m_1 (Fig. 5). The clustering analysis depicted sampling of more diverse conformations in baicalein compared to the control which is consistent with the RMSF analysis.

The visual inspection of the conformational snapshots of the control depicts the preservation of the LS-shaped morphology in the control; however, notable distortion from the initial structure was noted on incorporating baicalein and the structure became less ordered (Fig. 6).

The hydrophobic core constituted by F4, L34, and V36 stabilized the 5OQV LS-shaped topology.[7] A notable increase in the distance between the hydrophobic residues F4, L34, and V36 of the 5OQV structure upon inclusion of baicalein depicts reduced contacts among these residues leading to the distortions in the fibril assembly (Fig. S8, ESI†). Furthermore, visualization of the conformational snapshots depicts that the close contacts between hydrophobic residues F4, L34, and V36 of different chains of the 5OQV structure got disrupted by the incorporation of baicalein, indicating the destabilization of the protofibril structure (Fig. S8, ESI†).

3.4 Effect of baicalein on the kink angle and K28–A42 salt bridges in $A\beta_{42}$ protofibrils

The hydrogen bonds between H6–E11 and E11–H13 stabilize the kink angle around Y10 (L-shaped portion) while the salt bridge interactions between K28–A42 stabilize the S-shaped portion of protofibrils. The baicalein-induced structural divergence from the stable protofibril shape is reflected in the considerable increase in the kink angle. The average kink angle was noted to be $88.5^\circ \pm 0.4^\circ$ in the control. In contrast, the kink angle was notably increased to $96.2^\circ \pm 0.9^\circ$ in the presence of

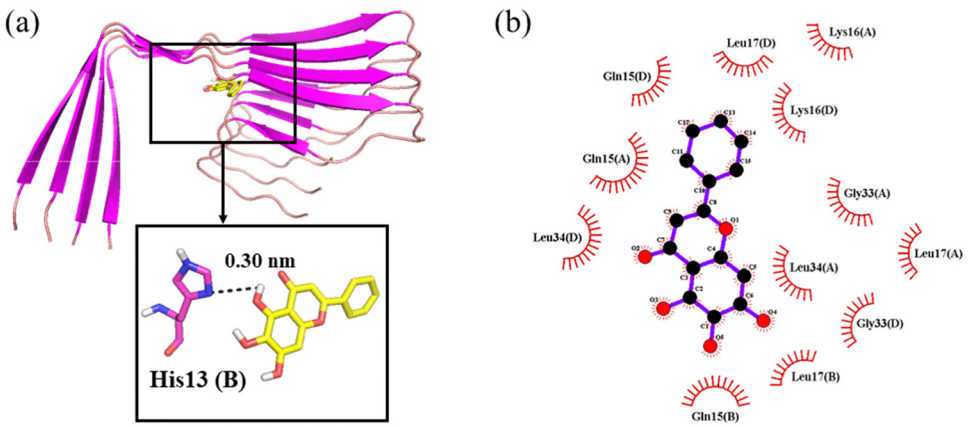

Fig. 5 Representative conformation of the most-populated microstate depicting a hydrogen bond between baicalein and His13 of chain B of the $A\beta_{42}$ protofibril (panel (a)). 2D map displaying the hydrophobic contacts of baicalein with $A\beta_{42}$ protofibrils in the representative conformation of the most-populated microstate (panel (b)).

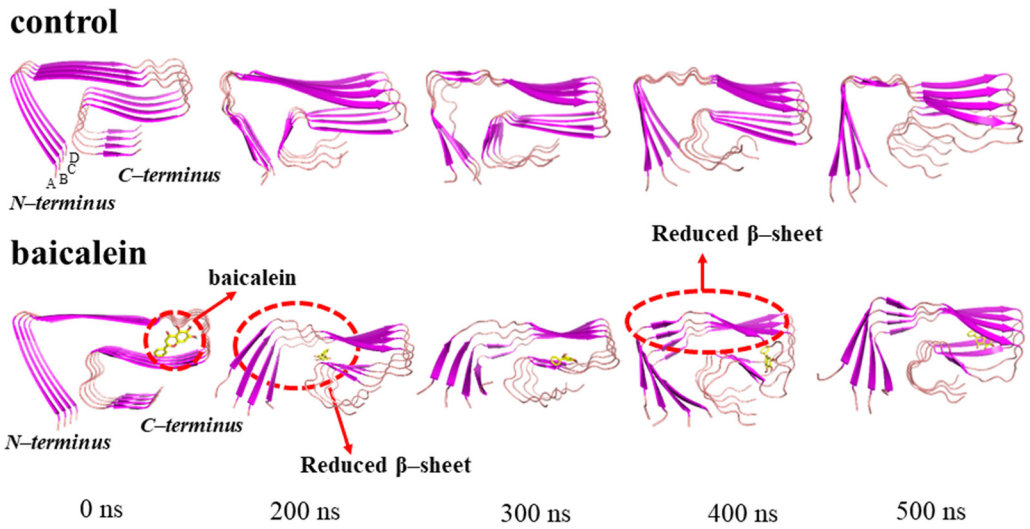

Fig. 6 Conformational snapshots of the MD trajectory of the control and baicalein systems depicting reduced sampling of β-sheets leading to the distortion in the protofibril chains in the baicalein system.

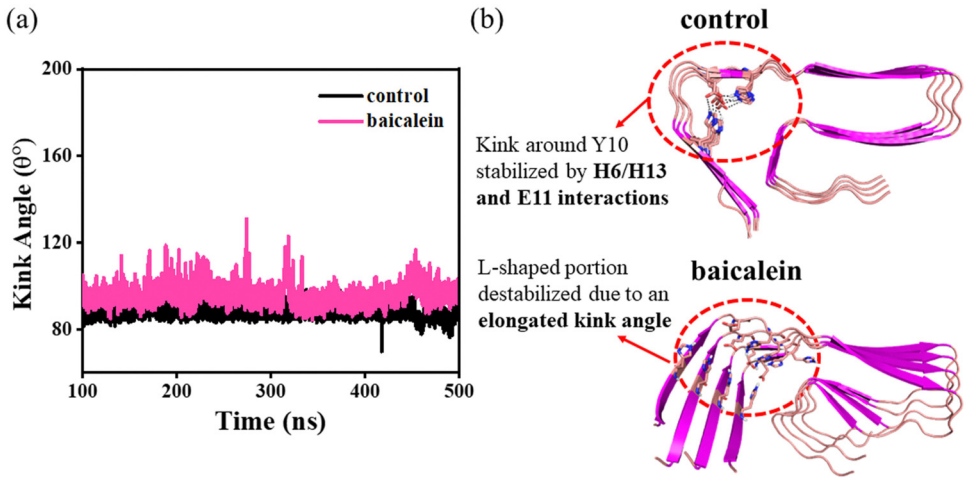

Fig. 7 Time-dependent variations in the kink angle between the H6–Y10 and Y10–H14 segments of $A\beta_{42}$ protofibrils with and without baicalein are shown in panel (a). Conformational snapshots depicting the distortion in the LS-shaped morphology of the 5OQV protofibril structure due to the elongation of the kink angle in the baicalein system are shown in panel (b).

baicalein (Fig. 7(a)), which indicates distortion in the L-shaped portion of the protofibrils. This is consistent with the conformational snapshots that demonstrate the kink angle dramatic transformation (Fig. 7(b)). Furthermore, the kink angle was increased in the different chains of the protofibrils upon incorporation of baicalein, as seen in the distribution curves of the kink angle (Fig. S9, ESI†), which, in turn, depicts a destabilization of the LS-shaped morphology of the protofibrils.

As the L-shaped portion of protofibrils is stabilized by the interactions among H6/H13 and E11 residues, the influence of baicalein on the H6–E11 and E11–H13 hydrogen bonds was examined (Table S3, ESI†). The average number of H6–E11 hydrogen bonds was noted to significantly decrease from 0.31 ± 0.10 in the control to 0.02 ± 0.01 in baicalein, whereas hydrogen bonds between E11–H13 increased from 0.25 ± 0.10 in the control to 0.33 ± 0.12 in baicalein. This is consistent with Zhan *et al.* depicting alternation in the H6–E11 and E11–H13 hydrogen bonds in $A\beta_{42}$ protofibrils (PDB ID: 5OQV) upon incorporation of EGCG and EGC.[24] Thus, modulation in the hydrogen bonds between H6/H13 and E11 residues depicts protofibril destabilization upon incorporation of baicalein.

The salt bridge interactions stabilize the $A\beta_{42}$ protofibril architecture.[6a,45] The $A\beta_{17-42}$,[45a] $A\beta_{9-40}$,[46] and $A\beta_{1-40}$[47] protofibrils with U-shaped structures are stabilized by K28–D23 salt bridges, whereas S-shaped[6] $A\beta_{11-42}$ and LS-shaped[7] $A\beta_{1-42}$ protofibrils are stabilized by salt bridge interactions between K28 and A42. The K28–A42 intrachain and interchain salt bridges in $A\beta_{42}$ protofibrils are affected by the incorporation of baicalein (Fig. 8 and Fig. S10, ESI†). The K28–A42 distances were noted to be 0.36, 0.47, 0.36, and 0.36 nm in chains A, B, C, and D,

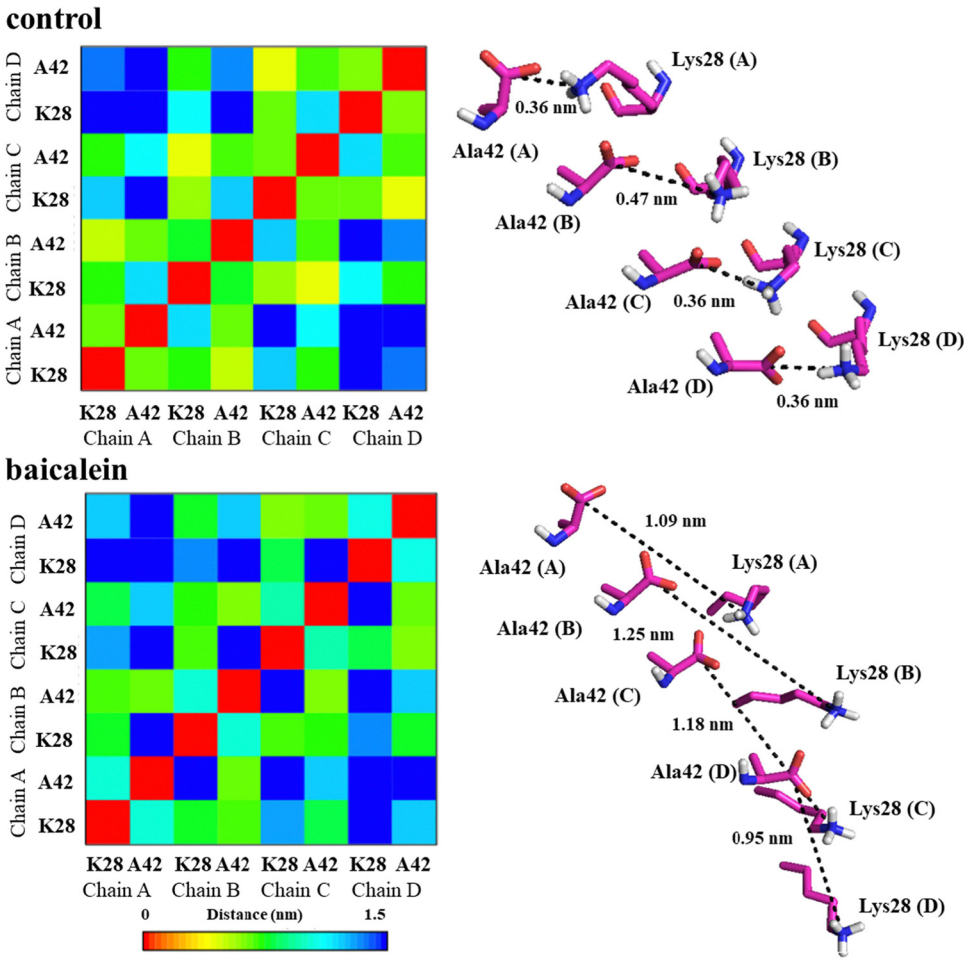

Fig. 8 Contact maps displaying the salt bridges between K28 (side chain NH_3^+) and A42 (C-terminal COO^-) in the control (upper panel) and baicalein (lower panel). The conformational snapshots display the intrachain salt bridge distance (nm) between K28–A42 in two systems.

respectively, of protofibrils in the control (Fig. 8(b)). In contrast, the intrachain salt bridge distances were significantly increased to 1.09, 1.25, 1.18, and 0.95 nm in chains A, B, C, and D, respectively, of the protofibrils on the incorporation of baicalein, which demonstrates the ability of baicalein to destabilize the protofibril structure by disrupting the K28–A42 salt bridge interactions, which are considered critical for the protofibril stability. The interchain salt bridges in the protofibril are partially destroyed and the disruption was noted to be less pronounced as compared to the intrachain salt bridges. This is consistent with Gong *et al.* depicting greater intrachain K28–A42 salt bridge disruption as compared to interchain salt bridges in the $A\beta_{42}$ protofibril (PDB ID: 5OQV) on the incorporation of melatonin and serotonin.[44]

3.5 Baicalein distorts $A\beta_{42}$ protofibrils by modulating side chain–side chain interactions and solvent-accessible surface area (SASA)

The side chain–side chain contacts were examined in the different chains of the $A\beta_{42}$ protofibrils on the incorporation of baicalein (Fig. 9). The LS-shaped morphology of $A\beta_{42}$ protofibrils is stabilized by three hydrophobic cores (A2, F4, L34, and V36 comprise core 1, core 2 is formed by contacts among L17, E19, and I31, while the contacts between A30, I32, M35, and V40 constitute core 3).[7] A large number of contacts were observed between the residues of hydrophobic core 1 region in chains A, B, C, and D of the $A\beta_{42}$ protofibril in the control (Fig. 9, upper panel). In contrast, these contacts were disrupted in all chains of the $A\beta_{42}$ protofibrils upon the incorporation of baicalein (Fig. 9, lower panel), which in turn depicts the destabilization of the $A\beta_{42}$ protofibrils. Furthermore, the contacts between residues of the hydrophobic core 2 region were affected in chains A and B of the $A\beta_{42}$ protofibrils on the addition of baicalein. Thus, contact map analysis highlighted the disruption of the hydrophobic contacts between core 1 and 2 residues in the presence of baicalein leading to the distortion in the $A\beta_{42}$ protofibrils.

To examine the impact of baicalein on the structural compactness of the $A\beta_{42}$ protofibril structure, SASA analysis was performed (Fig. 10). It is worth noting that the SASA value was increased from 104.32 ± 0.14 nm^2 in the control to 115.40 ± 0.15 nm^2 in the baicalein system, which highlights a disordered $A\beta_{42}$ protofibril structure with increased exposure to solvent water. This is consistent with Fang *et al.* depicting enhanced

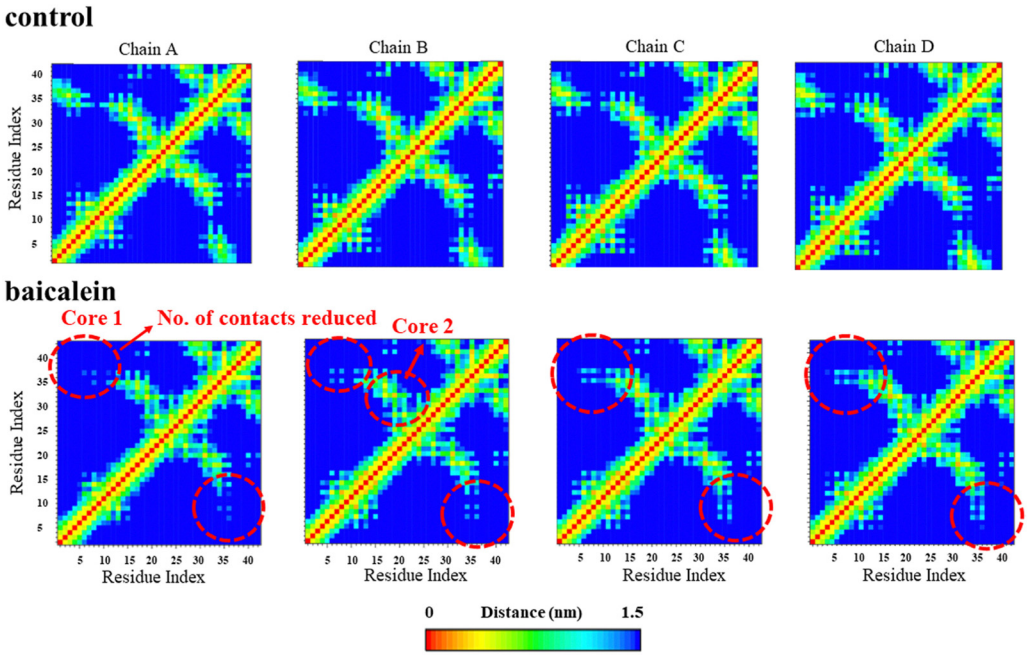

Fig. 9 Intrachain side chain–side chain contact map analysis in the control (upper panel) and baicalein systems (lower panel).

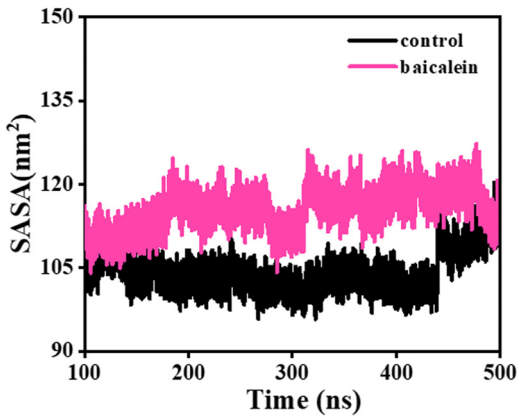

Fig. 10 Time-dependent variations in the SASA of the control and baicalein systems.

SASA in the complexes of the $A\beta_{42}$ protofibril (PDB ID: 5OQV) with licochalcone A and licochalcone B as compared to the $A\beta_{42}$ protofibril alone.[48]

3.6 Effect of baicalein on the conformational sampling in $A\beta_{42}$ protofibrils

The impact of baicalein on the distortion of the LS-shaped morphology of $A\beta_{42}$ protofibrils was examined using secondary structure analysis (Table 2). The β-sheet content was noted to be 60.7 ± 0.6% in the control, which is consistent with the value of 61.36 ± 0.31% in a protofibrillar structure (PDB ID: 5OQV) reported in a previous study.[49] Importantly, the β-sheet content was notably reduced from 60.7 ± 0.6% in the control to 56.7 ± 0.9% in baicalein with the coil content increasing from 25.7 ± 0.4% to 29.9 ± 0.7%. The reduced β-sheet content resulted in loosening of the chains, followed by protofibril distortion, which is consistent with the conversion of β-sheet rich neurotoxic Aβ oligomers into amorphous, off-pathway oligomeric species in the presence of resveratrol and EGCG.[50] The simulations with varying initial velocities depict an identical sampling of different secondary structures in the control and baicalein systems that highlight the consistency of the MD simulations (Table S4, ESI†).

Table 2 Secondary structure compositions for the control and baicalein systems

Secondary structure component	Control	Baicalein
β-sheet[a]	60.7 ± 0.6	56.7 ± 0.9
Coil	25.7 ± 0.4	29.9 ± 0.7
Bend	12.0 ± 0.0	11.2 ± 0.7
Turn	0.3 ± 0.2	0.0 ± 0.0
Chain separator	2.0 ± 0.0	2.0 ± 0.0

[a] β-sheet = β-strand + β-bridge.

Furthermore, notable lower sampling of the β-sheet content in Glu11, Val12, His13, Phe20, Ala21, Glu22, Val24, Gly25, Ser26, Asn27, Ala30, Ile31, Ile32, Gly33 and Leu34 of protofibrils with a concomitant increase in the coil content upon the incorporation of baicalein was observed (Fig. 11). Thus, baicalein primarily affects the β-sheet content of the CHC and C-terminal regions of $A\beta_{42}$, which, in turn, leads to disruption of the key interactions responsible for stabilizing the protofibril structure. This is consistent with Gong *et al.* depicting that serotonin decreased the β-sheet content in the N-terminal and melatonin decreased the β-sheet content in the C-terminal of

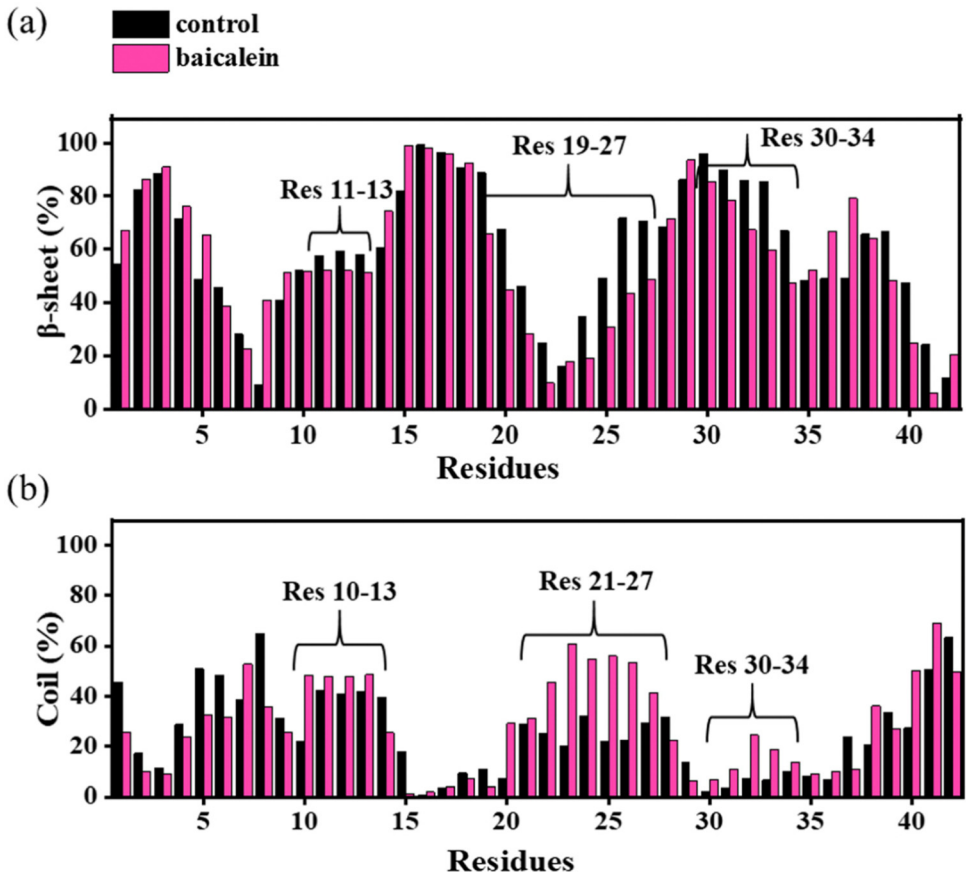

Fig. 11 Per-residue β-sheet (panel (a)) and coil (panel (b)) contents in the control and baicalein systems.

the $A\beta_{42}$ protofibril (PDB ID: 5OQV).[44] Thus, baicalein altered the LS-shaped morphology of $A\beta_{42}$ protofibrils by modulating the β-sheet and coil contents.

3.7 Baicalein decreases the interchain binding affinity in $A\beta_{42}$ protofibrils

Baicalein binds to the $A\beta_{42}$ protofibril with a binding free energy of -50.13 ± 4.18 kcal mol^{-1} (Table 3). The van der Waals ($\Delta E_{vdw} = -41.17 \pm 1.95$ kcal mol^{-1}) and non-polar solvation ($\Delta G_{nps} = -32.95 \pm 3.44$ kcal mol^{-1}) terms favour the binding of baicalein to the $A\beta_{42}$ protofibril, whereas polar solvation and electrostatic interactions are unfavourable.

Table 3 Binding free energy of baicalein with $A\beta_{42}$ protofibrils

Energy terms (kcal mol^{-1})	$A\beta_{42}$ protofibril–baicalein
ΔE_{vdW}	-41.17 ± 1.95
ΔE_{elec}	0.47 ± 0.93
ΔE_{MM}[a]	-40.70 ± 1.03
ΔG_{ps}	23.52 ± 1.73
ΔG_{nps}	-32.95 ± 3.44
ΔG_{solv}[b]	-9.43 ± 1.70
$\Delta G_{binding}$[c]	-50.13 ± 4.18

[a] $\Delta E_{MM} = \Delta E_{vdW} + \Delta E_{elec}$. [b] $\Delta G_{solv} = \Delta G_{ps} + \Delta G_{nps}$. [c] $\Delta G_{binding} = \Delta E_{MM} + \Delta G_{solv}$.

Furthermore, the per-residue binding free energy of the $A\beta_{42}$ protofibril residues with baicalein was evaluated (Fig. 12). Notably, Phe19(A) (−6.39), Ile31(A) (−1.37), Leu17(B) (−3.02), Glu29(B) (−1.69), Phe19(D) (−3.62), and Ile31(D) (−2.47) of the $A\beta_{42}$ protofibrils contributed significantly in the binding with baicalein. The toxic protein fibrillar aggregates are stabilized by hydrophobic contacts, hydrogen bonds, and π–π interactions, and interrupting these interactions will inhibit the self-aggregation of proteins to toxic oligomeric species.[51] Baicalein binds to CHC region residues (Leu17 and Phe19), which play a key role in the $A\beta_{42}$ self-assembly and subsequent stabilization of $A\beta_{42}$ aggregates.[43]

To assess the impact of baicalein on the interchain interactions in $A\beta_{42}$ protofibrils, interchain binding free energies were evaluated with and without baicalein (Table 4). Notably, the binding affinities were decreased from -143.96 ± 23.51 to -133.87 ± 18.89 for chain A–B, -142.15 ± 26.29 to -136.76 ± 19.10 for chain B–C, and -144.28 ± 24.64 to -118.26 ± 18.36 for chain C–D of $A\beta_{42}$ protofibrils on the inclusion of baicalein.

The average interchain binding free energy in the baicalein system was noted to be -129.63 ± 18.78 as compared to -143.46 ± 24.81 kcal mol^{-1} in the control, which depicts reduced interchain binding affinity leading to the distortion in the chains of $A\beta_{42}$ protofibrils as noted in the conformational snapshots.

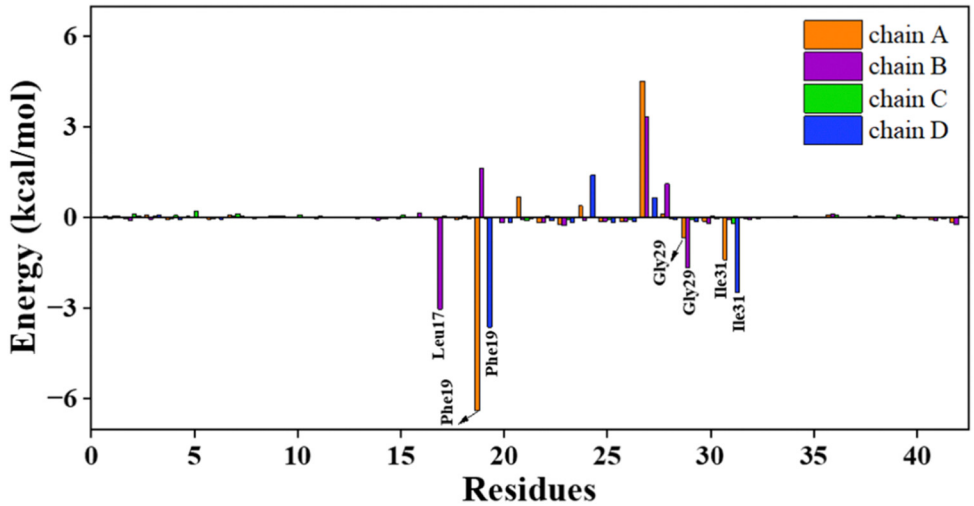

Fig. 12 Residue-wise contribution of the different chains of the protofibril to the binding free energy (kcal mol^{-1}) of the $A\beta_{42}$ protofibril–baicalein complex.

Table 4 Interchain binding free energy (kcal mol^{-1}) in $A\beta_{42}$ protofibrils in the absence and presence of baicalein

System	Chain	ΔE_{vdW}	ΔE_{elec}	ΔE_{MM} [a]	ΔG_{ps}	ΔG_{nps}	ΔG_{solv} [b]	$\Delta G_{binding}$ [c]
Control	A–B	−192.18 ± 6.13	28.93 ± 15.91	−163.27 ± 9.78	212.37 ± 29.49	−193.07 ± 10.88	19.29 ± 18.61	−143.96 ± 23.51
	B–C	−194.74 ± 6.39	42.29 ± 19.28	−152.46 ± 12.89	203.13 ± 33.75	−192.83 ± 10.64	10.29 ± 23.10	−142.15 ± 26.29
	C–D	−198.05 ± 8.81	44.17 ± 23.72	−153.88 ± 14.91	204.89 ± 35.11	−195.29 ± 12.17	9.69 ± 22.94	−144.28 ± 24.64
Baicalein	A–B	−189.54 ± 7.38	10.12 ± 18.52	−179.42 ± 11.15	237.52 ± 26.09	−191.97 ± 12.09	45.54 ± 13.99	−133.87 ± 18.89
	B–C	−190.99 ± 6.27	51.08 ± 14.14	−139.92 ± 7.87	190.85 ± 22.28	−187.69 ± 11.25	3.16 ± 11.25	−136.76 ± 19.10
	C–D	−191.87 ± 8.15	11.39 ± 18.69	−180.48 ± 10.54	250.96 ± 24.96	−188.74 ± 10.82	62.21 ± 14.13	−118.26 ± 18.36

[a] $\Delta E_{MM} = \Delta E_{vdW} + \Delta E_{elec}$. [b] $\Delta G_{solv} = \Delta G_{ps} + \Delta G_{nps}$. [c] $\Delta G_{binding} = \Delta E_{MM} + \Delta G_{solv}$.

4. Conclusions

In this work, extensive all-atom MD simulations have been performed to examine the molecular mechanism of baicalein-induced destabilization of LS-shaped $A\beta_{42}$ protofibrils. Notably, a higher conformational heterogeneity in protofibrils was observed with the addition of baicalein. Importantly, higher RMSF in $A\beta_{42}$ protofibril–baicalein depicts reduced structural stability leading to the destabilization of the protofibril structure. Binding free energy analysis using the MM-PBSA method depicted that baicalein binds favourably to protofibrils ($\Delta G_{binding}$ = −50.13 ± 4.18 kcal mol^{-1}) with the major contribution from the van der Waals interactions. Baicalein destabilizes the $A\beta_{42}$ protofibril by reducing the sampling of β-sheets, elongating the kink angle, and disrupting K28–A42 salt bridges, which are critical for the protofibril stability. This study illuminates the mechanism by which baicalein destabilizes $A\beta_{42}$ protofibrils and provides valuable insights into designing new, selective, and potent therapeutic candidates against protofibril destabilization in AD.

Conflicts of interest

There are no conflicts to declare.

Acknowledgements

BG acknowledges CSIR, India (Sanction No. 02(0451)/21/EMR-II), and SERB, India (Sanction No. CRG/2023/000088, CRG/2022/008244) for the financial support. The authors acknowledge Sri Guru Granth Sahib World University, Fatehgarh Sahib, India, and Thapar Institute of Engineering & Technology, Patiala, India, for the research infrastructure.

References

1 (*a*) A. Alzheimer, Über Eine Eigenartige Erkrankung Der Hirnrinde, *Allg. Z. Psychiatr. Psych.-Gerichtl. Med.*, 1907, **64**, 146–148; (*b*) H. Hippius and G. Neundörfer, The discovery of Alzheimer's disease, *Dialogues Clin. Neurosci.*, 2003, **5**, 101–108; (*c*) M. Goedert and M. G. Spillantini, A century of Alzheimer's disease, *Science*, 2006, **314**, 777–781; (*d*) M. A. DeTure and D. W. Dickson, The neuropathological diagnosis of Alzheimer's disease, *Mol. Neurodegener.*, 2019, **14**, 32; (*e*) P. H. Nguyen, A. Ramamoorthy, B. R. Sahoo, J. Zheng, P. Faller, J. E. Straub, L. Dominguez, J.-E. Shea, N. V. Dokholyan, A. De Simone, B. Ma, R. Nussinov, S. Najafi, S. T. Ngo, A. Loquet, M. Chiricotto, P. Ganguly, J. McCarty, M. S. Li, C. Hall, Y. Wang, Y. Miller, S. Melchionna,

B. Habenstein, S. Timr, J. Chen, B. Hnath, B. Strodel, R. Kayed, S. Lesné, G. Wei, F. Sterpone, A. J. Doig and P. Derreumaux, Amyloid oligomers: A joint experimental/computational perspective on Alzheimer's disease, Parkinson's disease, Type II diabetes, and Amyotrophic Lateral Sclerosis, *Chem. Rev.*, 2021, **121**, 2545–2647.

2 (*a*) **https://www.alzint.org/resource/attitudes-to-dementia-world-alzheimer-report-2024-survey-information/** (access date: May 12, 2024); (*b*) **https://www.who.int/news-room/fact-sheets/detail/dementia** (access date: May 12, 2024).

3 (*a*) D. Li and C. Liu, Molecular rules governing the structural polymorphism of amyloid fibrils in neurodegenerative diseases, *Structure*, 2023, **31**, 1335–1347; (*b*) S. H. W. Scheres, B. Ryskeldi-Falcon and M. Goedert, Molecular pathology of neurodegenerative diseases by cryo-EM of amyloids, *Nature*, 2023, **621**, 701–710; (*c*) S. Linse and T. Knowles, Amyloids and protein aggregation, *Chem. Sci.*, 2023, **14**, 6491–6492; (*d*) A. K. Buell, Stability matters, too–the thermodynamics of amyloid fibril formation, *Chem. Sci.*, 2022, **13**, 10177–10192.

4 J. Hardy and D. J. Selkoe, The amyloid hypothesis of Alzheimer's disease: Progress and problems on the road to therapeutics, *Science*, 2002, **297**, 353–356.

5 A. K. Paravastu, R. D. Leapman, W.-M. Yau and R. Tycko, Molecular structural basis for polymorphism in Alzheimer's β-amyloid fibrils, *Proc. Natl. Acad. Sci. U. S. A.*, 2008, **105**, 18349–18354.

6 (*a*) Y. Xiao, B. Ma, D. McElheny, S. Parthasarathy, F. Long, M. Hoshi, R. Nussinov and Y. Ishii, Aβ(1–42) fibril structure illuminates self–recognition and replication of amyloid in Alzheimer's disease, *Nat. Struct. Mol. Biol.*, 2015, **22**, 499–505; (*b*) P. H. Nguyen and P. Derreumaux, An S-shaped $A\beta_{42}$ cross-β hexamer embedded into a lipid bilayer reveals membrane disruption and permeability, *ACS Chem. Neurosci.*, 2023, **14**, 936–946; (*c*) N. G. Tung, P. Derreumaux, V. V. Vu, P. C. Nam and S. T. Ngo, C-terminal plays as the possible nucleation of the self-aggregation of the S-shape $A\beta_{11-42}$ tetramer in solution: Intensive MD study, *ACS Omega*, 2019, **4**, 11066–11073.

7 L. Gremer, D. Schölzel, C. Schenk, E. Reinartz, J. Labahn, R. B. G. Ravelli, M. Tusche, C. Lopez-Iglesias, W. Hoyer, H. Heise, D. Willbold and G. F. Schröder, Fibril structure of amyloid–β(1–42) by cryo–electron microscopy, *Science*, 2017, **358**, 116–119.

8 J. X. Lu, W. Qiang, W. Yau, C. D. Schwieters, S. C. Meredith and R. Tycko, Molecular structure of β-amyloid fibrils in Alzheimer's disease brain tissue, *Cell*, 2013, **154**, 1257–1268.

9 (*a*) R. Limbocker, N. Cremades, R. Cascella, P. M. Tessier, M. Vendruscolo and F. Chiti, Characterization of pairs of toxic and nontoxic misfolded protein oligomers elucidates the structural determinants of oligomer toxicity in protein misfolding diseases, *Acc. Chem. Res.*, 2023, **56**, 1395–1405; (*b*) A. J. Dear, G. Meisl, A. Šarić, T. C. T. Michaels, M. Kjaergaard, S. Linse and T. P. J. Knowles, Identification of on- and off-pathway oligomers in amyloid fibril formation, *Chem. Sci.*, 2020, **11**, 6236–6247; (*c*) S. J. Bunce, Y. Wang, K. L. Stewart, A. E. Ashcroft, S. E. Radford, C. K. Hall and A. J. Wilson, Molecular insights into the surface-catalyzed secondary nucleation of amyloid-β_{40} ($A\beta_{40}$) by the peptide fragment $A\beta_{16-22}$, *Sci. Adv.*, 2019, **5**, eaav8216.

10 (*a*) Y. Tang, D. Zhang and J. Zheng, Repurposing antimicrobial protegrin-1 as a dual-function amyloid inhibitor *via* cross-seeding, *ACS Chem. Neurosci.*, 2023, **14**, 3143–3155; (*b*) Y. Wang, J. Xu, F. Huang, J. Yan, X. Fan, Y. Zou, C. Wang, F. Ding and Y. Sun, SEVI inhibits Aβ amyloid aggregation by capping the β-sheet elongation edges, *J. Chem. Inf. Model.*, 2023, **63**, 3567–3578; (*c*) K. A. Murray, C. J. Hu, S. L. Griner and D. S. Eisenberg, De novo designed protein inhibitors of amyloid aggregation and seeding, *Proc. Natl. Acad. Sci. U. S. A.*, 2022, **119**, e2206240119; (*d*) M. Wu, L. Dorosh, G. Schmitt-Ulms, H. Wille and M. Stepanova, Aggregation of $A\beta_{40/42}$ chains in the presence of cyclic neuropeptides investigated by molecular dynamics simulations, *PLoS Comput. Biol.*, 2021, **17**, e1008771.

11 (*a*) E. McDade, J. L. Cummings, S. Dhadda, C. J. Swanson, L. Reyderman, M. Kanekiyo, A. Koyama, M. Irizarry, L. D. Kramer and R. J. Bateman, Lecanemab in patients with early Alzheimer's disease: Detailed results on biomarker, cognitive, and clinical effects from the randomized and open–label extension of the phase 2 proof–of–concept study, *Alzheimer's Res. Ther.*, 2022, **14**, 191; (*b*) C. H. Dyck, C. J. Swanson, P. Aisen, R. J. Bateman, C. Chen, M. Gee, M. Kanekiyo, D. Li, L. Reyderman, S. Cohen, L. Froelich, S. Katayama, M. Sabbagh, B. Vellas, D. Watson, S. Dhadda, M. Irizarry, L. D. Kramer and T. Iwatsubo, Lecanemab in early Alzheimer's disease, *N. Engl. J. Med.*, 2023, **388**, 9–21.

12 (*a*) R. Roy and S. Paul, Illustrating the effect of small molecules derived from natural resources on amyloid peptides, *J. Phys. Chem. B*, 2023, **127**, 600–615; (*b*) Y.-L. Han, H.-H. Yin, C. Xiao, M. T. Bernards, Y. He and Y.-X. Guan, Understanding the molecular mechanisms of polyphenol inhibition of amyloid β aggregation, *ACS Chem. Neurosci.*, 2023, **14**, 4051–4061; (*c*) M. Fang, X. Wang, K. Su, X. Jia, P. Guan and X. Hu, Inhibition effect and molecular mechanisms of quercetin on the $A\beta_{42}$ dimer: A molecular dynamics simulation study, *ACS Omega*, 2023, **8**, 18009–18018; (*d*) N. Zhang, C. Yan, C. Yin, X. Hu, P. Guan and Y. Cheng, Structural remodeling mechanism of the toxic amyloid fibrillary mediated by epigallocatechin-3-gallate, *ACS Omega*, 2022, **7**, 48047–48058; (*e*) M. H. Dehabadi, A. Caflisch, L. M. Ilie and R. Firouzi, Interactions of curcumin's degradation products with the $A\beta_{42}$ dimer: A computational study, *J. Phys. Chem. B*, 2022, **126**, 7627–7637; (*f*) S. Brogi, H. Sirous, V. Calderone and G. Chemi, Amyloid β fibril disruption by oleuropein aglycone: long-time molecular dynamics simulation to gain insight into the mechanism of action of this polyphenol from extra virgin olive oil, *Food Funct.*, 2020, **11**, 8122–8132; (*g*) Y. Porat, A. Abramowitz and E. Gazit, Inhibition of amyloid fibril formation by polyphenols: Structural similarity and aromatic interactions as a common inhibition mechanism, *Chem. Biol. Drug Des.*, 2006, **67**, 27–37.

13 J. H. Lu, M. T. Ardah, S. S. K. Durairajan, L. F. Liu, L. X. Xie, W. F. D. Fong, M. Y. Hasan, J. D. Huang, O. M. A. El-Agnaf and M. Li, Baicalein inhibits formation of α-Synuclein oligomers within living cells and prevents Aβ peptide fibrillation and oligomerisation, *ChemBioChem*, 2011, **12**, 615–624.

14 (*a*) Q. Hu, V. N. Uversky, M. Huang, H. Kang, F. Xu, X. Liu, L. Lian, Q. Liang, H. Jiang, A. Liu, C. Zhang, F. Pan-Montojo and S. Zhu, Baicalein inhibits α–synuclein oligomer formation and prevents progression of α–synuclein accumulation in a rotenone mouse model of Parkinson's disease, *Biochim. Biophys. Acta Mol. Basis Dis.*, 2016, **1862**, 1883–1890; (*b*) M. Zhu, S. Rajamani, J. Kaylor, S. Han, F. Zhou and A. L. Fink, The flavonoid baicalein inhibits fibrillation of α-synuclein and disaggregates existing fibrils, *J. Biol. Chem.*, 2004, **279**, 26846–26857.

15 N. K. Bhatia, P. Modi, S. Sharma and S. Deep, Quercetin and baicalein act as potent antiamyloidogenic and fibril destabilizing agents for SOD1 fibrils, *ACS Chem. Neurosci.*, 2020, **11**, 1129–1138.

16 N. A. Fazili, I. A. Bhat, W. F. Bhat and A. Naeem, Antifibrillation propensity of a flavonoid baicalein against the fibrils of hen egg white lysozyme: Potential therapeutics for lysozyme amyloidosis, *J. Biomol. Struct. Dyn.*, 2016, **34**, 2102–2114.

17 S. M. Song, Y. X. Wang, L. M. Xiong, L. B. Qu and M. T. Xu, AFM and fluorescence spectroscopy investigation for disaggregation of existing Aβ fibrils by baicalein, *Chin. Chem. Lett.*, 2012, **23**, 595–598.

18 X.-H. Gu, L.-J. Xu, Z.-Q. Liu, B. Wei, Y.-J. Yang, G.-G. Xu, X.-P. Yin and W. Wang, The flavonoid baicalein rescue synaptic plasticity and memory deficits in a mouse model of Alzheimer's disease, *Behav. Brain Res.*, 2016, **311**, 309–321.

19 (*a*) Y. Chen, C. Zhan, X. Li, T. Pan, Y. Yao, Y. Tan and G. Wei, Five similar anthocyanidin molecules display distinct disruptive effects and mechanisms of action on $A\beta_{1-42}$ protofibril: A molecular dynamic simulation study, *Int. J. Biol. Macromol.*, 2024, **256**, 128467; (*b*) X. Li, Y. Zhang, Y. Wang, S. Zhang and L. Zhang, Molecular insights into the inhibition and disaggregation effects of EGCG on Aβ40 and Aβ42 cofibrillation, *J. Phys. Chem. B*, 2024, **128**, 1843–1853; (*c*) A. A. Mohammed, S. S. Barale, S. A. Kamble, S. B. Paymal and K. D. Sonawane, Molecular insights into the inhibition of early stages of Aβ peptide aggregation and destabilization of Alzheimer's Aβ protofibril by dipeptide D-Trp-Aib: A molecular modelling approach, *Int. J. Biol. Macromol.*, 2023, **242**, 124880; (*d*) C. Zhan, Z. Lao, Y. Tang, Q. Qiao and G. Wei, Natural stereoisomeric flavonoids exhibit different disruptive effects and the mechanism of action on $A\beta_{42}$ protofibril, *Chem. Commun.*, 2021, **57**, 4267–4270; (*e*) A. Kaur, S. Shuaib, D. Goyal and B. Goyal, Interactions of a multifunctional di-triazole derivative with Alzheimer's $A\beta_{42}$ monomer and $A\beta_{42}$ protofibril: A systematic molecular dynamics study, *Phys. Chem. Chem. Phys.*, 2020, **22**, 1543–1556; (*f*) H. M. Hung, M. T. Nguyen, P. Tran, V. K. Truong, J. Chapman, L. H. Q. Anh, P. Derreumaux, V. V. Vu and S. T. Ngo, Impact of the astaxanthin, betanin, and EGCG compounds on small oligomers of amyloid $A\beta_{40}$ peptide, *J. Chem. Inf. Model.*, 2020, **60**, 1399–1408; (*g*) Z. Liu, Y. Zou, Q. Zhang, P. Chen, Y. Liu and Z. Qian, Distinct binding dynamics, sites and interactions of fullerene and fullerenols with amyloid-β peptides revealed by molecular dynamics simulations, *Int. J. Mol. Sci.*, 2019, **20**, 2048; (*h*) P. H. Nguyen, M. P. del Castillo-Frias, O. Berthoumieux, P. Faller, A. J. Doig and P. Derreumaux, Amyloid-β/drug interactions from computer simulations and cell-based assays, *J. Alzheimer's Dis.*, 2018, **64**, S659–S672; (*i*) L. Tran, J. Kaffy, S. Ongeri and T. Ha-Duong, Binding modes of a glycopeptidomimetic molecule on Aβ protofibrils: Implication for its inhibition mechanism, *ACS Chem. Neurosci.*, 2018, **9**, 2859–2869.

20 Q. Wang, X. Yu, K. Patal, R. Hu, S. Chuang, G. Zhang and J. Zheng, Tanshinones inhibit amyloid aggregation by amyloid–β peptide, disaggregate amyloid fibrils, and protect cultured cells, *ACS Chem. Neurosci.*, 2013, **4**, 1004–1015.

21 Y. Wang, D. C. Latshaw and C. K. Hall, Aggregation of Aβ(17–36) in the presence of naturally occurring phenolic inhibitors using coarse–grained simulations, *J. Mol. Biol.*, 2017, **429**, 3893–3908.

22 T. D. Martin, A. J. Malagodi, E. Y. Chi and D. G. Evans, A computational study of the driving forces and dynamics of curcumin binding to amyloid–β protofibrils, *J. Phys. Chem. B*, 2019, **123**, 551–560.

23 S. Gupta and A. K. Dasmahapatra, Caffeine destabilizes preformed Aβ protofilament: Insights from all atom molecular dynamics simulations, *Phys. Chem. Chem. Phys.*, 2019, **21**, 22067–22080.

24 C. Zhan, Y. Chen, Y. Tang and G. Wei, Green tea extracts EGCG and EGC display distinct mechanisms in disrupting $A\beta_{42}$ protofibril, *ACS Chem. Neurosci.*, 2020, **11**, 1841–1851.

25 K. Ono, D. B. Teplow, M. Condron and M. Yamada, Structure-neurotoxicity relationships of amyloid beta-protein oligomers, *Proc. Natl. Acad. Sci. U. S. A.*, 2009, **106**, 14745–14750.

26 W. L. DeLano, *The PyMOL molecular graphics system*, Delano Scientific, San Carlos, CA, 2002.

27 R. A. Laskowski and M. B. Swindells, LigPlot+: Multiple ligand–protein interaction diagrams for drug discovery, *J. Chem. Inf. Model.*, 2011, **51**, 2778–2786.

28 K. Lindorff-Larsen, S. Piana, K. Palmo, P. Maragakis, J. L. Klepeis, R. O. Dror and D. E. Shaw, Improved side–chain torsion potentials for the Amber ff99SB protein force field, *Proteins: Struct., Funct., Bioinf.*, 2010, **78**, 1950–1958.

29 (*a*) M. J. Abraham, T. Murtola, R. Schulz, S. Pall, J. C. Smith, B. Hess and E. Lindahl, GROMACS: High performance molecular simulations through multi-level parallelism from laptops to supercomputers, *SoftwareX*, 2015, **1–2**, 19–25; (*b*) D. van der Spoel, E. Lindahl, B. Hess, G. Groenhof, A. E. Mark and H. J. C. Berendsen, GROMACS: Fast, flexible, and free, *J. Comput. Chem.*, 2005, **26**, 1701–1718; (*c*) H. J. C. Berendsen, D. van der Spoel and R. van Drunen, GROMACS: A message–passing parallel molecular dynamics implementation, *Comput. Phys. Commun.*, 1995, **91**, 43–56.

30 K. A. Malde, L. Zuo, M. Breeze, M. Stroet, D. Poger, C. P. Nair, C. Oostenbrink and E. A. Mark, An automated force field topology builder (ATB) and repository: Version 1.0, *J. Chem. Theory Comput.*, 2011, **7**, 4026–4037.

31 (*a*) H. Bhagavatula, A. Sarkar, B. Santra and A. Das, Scan-find-scan-model: Discrete site-targeted suppressor design strategy for amyloid–β, *ACS Chem. Neurosci.*, 2022, **13**, 2191–2208; (*b*) P. Khatua, A. K. Jana and U. H. E. Hansmann, Effect of lauric acid on the stability of $A\beta_{42}$ Oligomers, *ACS Omega*, 2021, **6**, 5795–5804.

32 W. L. Jorgensen, J. Chandrasekhar, J. D. Madura, R. W. Impey and M. L. Klein, Comparison of simple potential functions for simulating liquid water, *J. Chem. Phys.*, 1983, **79**, 926–930.

33 (*a*) T. Darden, D. York and L. Pedersen, Particle mesh Ewald: An N·log (N) method for Ewald sums in large systems, *J. Chem. Phys.*, 1993, **98**, 10089–10092; (*b*) U. Essmann, L. Perera and M. L. Berkowitz, A smooth particle mesh Ewald method, *J. Chem. Phys.*, 1995, **103**, 8577–8593.

34 (*a*) M. Parrinello and A. Rahman, Polymorphic transitions in single crystals: A new molecular dynamics method, *J. Appl. Phys.*, 1981, **52**, 7182–7190; (*b*) A. Rahman and F. H. Stillinger, Molecular dynamics study of liquid water, *J. Chem. Phys.*, 1971, **55**, 3336–3359.

35 G. Bussi, D. Donadio and M. Parrinello, Canonical sampling through velocity rescaling, *J. Chem. Phys.*, 2007, **126**, 014101.

36 W. Kabsch and C. Sander, Dictionary of protein secondary structure: Pattern recognition of hydrogen–bonded and geometrical features, *Biopolymers*, 1983, **22**, 2577–2637.

37 (*a*) X. Daura, K. Gademann, B. Jaun, D. Seebach, W. F. van Gunsteren and A. E. Mark, Peptide folding: When simulation meets experiment, *Angew. Chem., Int. Ed.*, 1999, **38**, 236–240; (*b*) L. J. Smith, X. Daura and W. F. van Gunsteren, Assessing equilibration and convergence in biomolecular simulations, *Proteins: Struct., Funct., Bioinf.*, 2002, **48**, 487–496.

38 (*a*) S. Genheden and U. Ryde, The MM/PBSA and MM/GBSA methods to estimate ligand–binding affinities, *Expert Opin. Drug Discovery*, 2015, **10**, 449–461; (*b*) R. Kumari and R. Kumar, g_mmpbsa—A GROMACS tool for high–throughput MM–PBSA calculations, *J. Chem. Inf. Model.*, 2014, **54**, 1951–1962.

39 (*a*) B. Han, Y. Liu, W. S. Ginzinger and S. D. Wishart, SHIFTX2: Significantly improved protein chemical shift prediction, *J. Biomol. NMR*, 2011, **50**, 43–57; (*b*) S. Neal, A. M. Nip, H. Zhang and D. S. Wishart, Rapid and accurate calculation of protein ^{1}H, ^{13}C and ^{15}N chemical shifts, *J. Biomol. NMR*, 2003, **26**, 215–240.

40 **https://bmrb.io/data_library/summary/?bmrbid=27212**, DOI: **10.13018/BMR27212**.

41 A. Kaur, D. Goyal and B. Goyal, An α-helix mimetic oligopyridylamide, ADH–31, modulates $A\beta_{42}$ monomer aggregation and destabilizes protofibril structures: Insights from molecular dynamics simulations, *Phys. Chem. Chem. Phys.*, 2020, **22**, 28055–28073.

42 J. T. Jarrett, E. P. Berger and P. T. Lansbury Jr, The carboxy terminus of the amyloid protein is critical for the seeding of amyloid formation: Implications for the pathogenesis of Alzheimer's disease?, *Biochemistry*, 1993, **32**, 4693–4697.

43 (*a*) P. P. Mager and K. Fischer, Simulation of the lipophilic and antigenic cores of the Aβ(1-42) peptide of Alzheimer's disease, *Mol. Simul.*, 2001, **27**, 237–242; (*b*) L. O. Tjernberg, J. Näslund, F. Lindqvist, J. Johansson, A. R. Karlström, J. Thyberg, L. Terenius and C. Nordstedt, Arrest of β-amyloid fibril formation by a pentapeptide ligand, *J. Biol. Chem.*, 1996, **271**, 8545–8548; (*c*) A. Jarmuła, M. Zubalska and D. Stępkowski, Consecutive aromatic residues are required for improved efficacy of β-sheet breakers, *Int. J. Mol. Sci.*, 2022, **23**, 5247; (*d*) K. Watanabe, T. Segawa, K. Nakamura, M. Kodaka, T. Konakahara and H. Okuno, Identification of the molecular interaction site of amyloid β peptide by using a fluorescence assay, *J. Pept. Res.*, 2001, **58**, 342–346; (*e*) A. Jarmuła, J. Ludwiczak and D. Stępkowski, β-sheet breakers with consecutive phenylalanines: Insights into mechanism of dissolution of β-amyloid fibrils, *Proteins: Struct., Funct., Bioinf.*, 2021, **89**, 762–780.

44 Y. Gong, C. Zhan, Y. Zou, Z. Qian, G. Wei and Q. Zhang, Serotonin and melatonin show different modes of action on $A\beta_{42}$ protofibril destabilization, *ACS Chem. Neurosci.*, 2021, **12**, 799–809.

45 (*a*) T. Lührs, C. Ritter, M. Adrian, D. Riek-Loher, B. Bohrmann, H. Döbeli, D. Schubert and R. Riek, 3D structure of Alzheimer's amyloid–β (1–42) fibrils, *Proc. Natl. Acad. Sci. U. S. A.*, 2005, **102**, 17342–17347; (*b*) D. Thirumalai, D. Klimov and R. Dima, Emerging ideas on the molecular basis of protein and peptide aggregation, *Curr. Opin. Struct. Biol.*, 2003, **13**, 146–159.

46 R. Tycko, Progress towards a molecular–level structural understanding of amyloid fibrils, *Curr. Opin. Struct. Biol.*, 2004, **14**, 96–103.

47 A. T. Petkova, W. M. Yau and R. Tycko, Experimental constraints on quaternary structure in Alzheimer's β–amyloid fibrils, *Biochemistry*, 2006, **45**, 498–512.

48 M. Fang, K. Su, X. Wang, P. Guan and X. Hu, Study on molecular mechanisms of destabilizing Aβ(1–42) protofibrils by licochalcone A and licochalcone B using molecular dynamics simulations, *J. Mol. Graph. Model.*, 2023, **122**, 108500.

49 D. Gao, J. Wan, Y. Zou, Y. Gong, X. Dong, Z. Xu, J. Tang, G. Wei and Q. Zhang, The destructive mechanism of $A\beta_{1-42}$ protofibrils by norepinephrine revealed via molecular dynamics simulations, *Phys. Chem. Chem. Phys.*, 2022, **24**, 19827–19836.

50 F. Li, C. Zhan, X. Dong and G. Wei, Molecular mechanisms of resveratrol and EGCG in the inhibition of $A\beta_{42}$ aggregation and disruption of $A\beta_{42}$ protofibril: Similarities and differences, *Phys. Chem. Chem. Phys.*, 2021, **23**, 18843–18854.

51 (*a*) E. Gazit, A possible role for π-stacking in the self-assembly of amyloid fibrils, *FASEB J.*, 2002, **16**, 77–83; (*b*) R. Scherzer-Attali, R. Pellarin, M. Convertino, A. Frydman-Marom, N. Egoz-Matia, S. Peled, M. Levy-Sakin, D. E. Shalev, A. Caflisch, E. Gazit and D. Segal, Complete phenotypic recovery of an Alzheimer's disease model by a quinone-tryptophan hybrid aggregation inhibitor, *PLoS One*, 2010, **5**, e11101.

